IEEE Access
Multidisciplinary | Rapid Review | Open Access Journal

Received 8 November 2023, accepted 5 December 2023, date of publication 13 December 2023,
date of current version 18 December 2023.

Digital Object Identifier 10.1109/ACCESS.2023.3342322

RESEARCH ARTICLE

Nonlinear Dynamics of Pilot-Operated Hydraulic Control Valves for Submersible Based on Improved Newmark-β Integration Method

SHUXUN LI[1], YU ZHANG[1], CHAO LIAN[2], AND JIANJUN HOU[1]
[1]School of Petrochemical Engineering, Lanzhou University of Technology, Lanzhou 730050, China
[2]Shanghai Institute of Applied Physics, Chinese Academy of Sciences, Shanghai 201800, China

Corresponding author: Yu Zhang (17361568493@163.com)

This work was supported in part by the National Natural Science Foundation of China through the Research Project under Grant 51569012, in part by the Double First-Class Key Program of Gansu Provincial Department of Education, and in part by the Gansu Province Science and Technology Program under Grant 22CX8GA125.

ABSTRACT Submersible is an important equipment for the development and utilization of marine resources. The pilot-operated hydraulic control valves have an extremely wide range of applications in the buoyancy adjustment system of submersibles. The existing hydraulic control valves have insufficient flow rate and pressure adjustment ability in a wide range of system pressures. A pilot-operated hydraulic control valve with a wide range of adjustable pressures, a high flow rate control accuracy, and anti-turbulence and cavitation is designed. A joint simulation method combining MATLAB/Simulink and UDF dynamic mesh is developed. The dynamic characteristics of the piping system and pilot-operated hydraulic control valve under different system inlet pressures are investigated by using the metric cellular automata technology and one- and three-dimensional co-simulation platforms. The results of the joint simulation show that: the flow rate of the system stabilizes for a period at a system inlet pressure of 1.6 MPa, and the phenomena such as fluctuations and oscillations will occur after a period. To address this phenomenon, an improved Newmark-β integration method is proposed based on establishing a correct nonlinear model. The established model is solved in a longer time domain to obtain the nonlinear dynamic bifurcation behavior of the model. The stability of the pilot-operated hydraulic control valve is analyzed by displacement dynamic response diagrams, phase space trajectory diagrams, and bifurcation diagrams. A direction is provided for the applied research of nonlinear system bifurcation theory in self-operated valves.

INDEX TERMS Cellular automata, dynamic characterization, improved Newmark-β integration method, pilot-hydraulic control valve, stability, submersible.

I. INTRODUCTION

Submersible is an important equipment for the exploitation and utilization of marine resources. As the core subsystem of the submersible, the buoyancy adjustment system is used to control the weight and buoyancy of the submersible to realize the functions of hovering, depth fixing and compensating buoyancy changes [1]. Hydraulic control valves have a wide range of applications in the buoyancy regulation system, and are the key equipment for regulating the flow and pressure of the system to ensure that the submersible can dive and float normally. Hydraulic control valves play a vital role in stabilizing system performance and reducing energy consumption. Hydraulic control valves can be viewed as a nonlinear dynamic system under external disturbances. As the pressure rises, the vibration destabilization problem of the valve becomes more and more prominent, and it becomes one of the important problems for the safe supply of the buoyancy regulation system. If the vibration instability problem of the hydraulic control valve occurs, the pressure and

The associate editor coordinating the review of this manuscript and approving it for publication was Padmanabh Thakur.

flow rate of the system pipeline will not be guaranteed, and the safety of the pressure-resistant water compartment in the buoyancy adjustment system, and the submerged state of the submersible will be seriously affected [2], [3].

Theoretical models were developed [4], the use of MATLAB/Simulink system control equations were nonlinearly solved. equations were solved nonlinearly, and it was obtained that the root cause of the valve vibration is the leakage of the valve seal. The dynamic model of the check valve was established [5]. The dynamic characteristics of the outlet valve of the piston pump are calculated, and the study shows that the check valve converges at different crank speeds, but there is some closing hysteresis. The dependence of the working fluid supply on its basic slide valve differential pressure and on the parametric loading pressure is plotted [6]. Transient processes in the hydraulic drive control system are analyzed. A metric automata model is proposed for locating leaks in gas main drainage pipelines. The pressure distribution along the pipeline is predicted using flow and pressure parameters at both ends of the pipeline. The pipeline fluid is assumed to vary continuously in time and space, which improves the localization accuracy [7]. The nonlinear pressure loss between the orifice plate and the gap is analyzed by using the delay element [8]. The results show that the viscosity change of the fluid shows steady-state response results and transient response results.

Hydraulic control valve if vibration instability problems, the system pipeline pressure and flow will not be able to ensure that the buoyancy adjustment system in the pressure-resistant water cabin safety, submersible dive down state will be seriously affected. At present, many scholars have made many contributions to bifurcation characteristics [9], [10], [11], [12], [13]. But the self-operated valve on its nonlinear dynamic system bifurcation characteristics and stability of the application of research is very little, for the bifurcation characteristics of the relevant research is still mostly in the theoretical state.

A two-parameter bifurcation analysis of the mathematical model reveals that the valve instability is subcritical and that large amplitude shock chaotic motions and stable equilibrium operation can coexist [14]. The dynamics of a single-stage relief valve in a hydraulic circuit is modeled. The mechanism of valve destabilization was investigated using the Hopf bifurcation method, considering the compressibility of the fluid as well as the possible jerky behavior of the valve cone colliding with the valve seat. The mechanism of valve destabilization is investigated [15]. The stability of a doubly-fed variable-speed pump-turbine regulation system under low-power disturbance conditions is investigated [16]. The algebraic stability criterion of the system in turbine and pump modes is derived using Hopf bifurcation theory [17]. The equilibrium point of the system is analyzed and the conditions for Hopf bifurcation of the system are given [18]. Types of bifurcations are studied. The robustness and effectiveness of the controller of the system in the presence of parametric perturbations or additive feedback control perturbations are analyzed. Considering the axial and longitudinal vibration shocks between the spool and the valve seat, the structural parameters of the direct-acting relief valve were optimized and analyzed for reliability by means of an optimized closed loop composed of three algorithmic designs, and it was found that the axial vibration shock oscillations of the spool were responsible for the drastic fluctuations of the pump pressure [19]. A physical model of the relief valve is presented, and linear stability and Lyapunov exponential analyses are carried out [20]. Hopf bifurcation, generalized Hopf bifurcation and cusp bifurcation are found to exist in the piping system. The dynamic characteristics of the pilot operated relief valve were investigated using frequency domain analysis, and the local stability of the relief valve under different annular space gaps was investigated using the normalization method. It is found that the size of the piston-to-case gap has a significant effect on the local stability of the relief valve [21]. A nonlinear dynamics model of the actuator system dynamics was developed and the effect of the spool geometry on the bifurcation point of the system was investigated [22]. It was found that the spool geometry affects the flow characteristics of the spool and reduces the stabilization region of the spool parameter plane. A nonlinear dynamic model of the pilot-valve-controlled hydraulic system is established [23]. The bifurcation analysis method when the diameter of the feedback hole changes is proposed, and the stability of the system is analyzed. Participated in MATLAB/Simulink for nonlinear modeling and simulation of pilot operated relief valve [24]. The established models for predicting performance parameters under steady state and transient operating conditions were experimentally validated.

For the current research on the bifurcation characteristics and stability of the nonlinear dynamic system of the self-operated valve is very little. Most of the related research on the bifurcation characteristics is still in the theoretical state. The research on the dynamic characteristics of hydraulic control valves is also relatively limited. Most of them are studied from the perspective of mechanical equilibrium using one-dimensional dynamic characteristics simulation software, with relatively low simulation accuracy.

In this paper, the nonlinear dynamics of pilot operated hydraulic control valves is investigated using the improved Newmark-β integration method. The aim is to verify the feasibility of the improved Newmark-β integration method through the bifurcation principle. The main contributions of this paper are as follows:

1) A pilot operated hydraulic control valve with a wide adjustable pressure range, high flow control accuracy, and anti-turbulence and cavitation is designed, which is mainly used in the buoyancy adjustment system of submersibles, and the dynamic performance of the pilot operated hydraulic control is verified through simulation analysis.

2) A joint simulation method of MATLAB/Simulink and UDF dynamic mesh is developed, and the dynamic

characteristics of piping system and pilot-operated hydraulic control valve under different system inlet pressures are investigated by combining with the technique of meta-cellular automata.

3) An improved Newmark-β integration method is proposed to obtain the nonlinear dynamic bifurcation behavior of the model and analyze the stability of the system. This study provides a direction for the applied research of nonlinear system bifurcation theory in self-operated valves.

4)This study Nonlinear dynamics of pilot-operated hydraulic control valves for submersible based on improved Newmark-β integration method, through the in-depth study of nonlinear dynamics of hydraulic control valves, provides theoretical guidance to improve the design of submersibles, enhance the operating efficiency, safety, and reliability of submersibles, and promotes the collection and development of deep-sea mineral resources.

II. MODELING OF THE BUOYANCY ADJUSTMENT SYSTEM

A. MODELING OF BUOYANCY ADJUSTMENT SYSTEMS AND PILOT-OPERATED HYDRAULIC CONTROL VALVES

The buoyancy adjustment system is used to control the weight and buoyancy of the submersible to realize the functions of hovering, depth fixing and buoyancy change compensation. As shown in Fig. 1, the buoyancy adjustment system of the submersible consists of pressure-resistant tank, inlet filter, throttling orifice, pilot hydraulic control valve, shut-off valve, regulating valve, through-sea filter, check valve and regulating ball valve. As the dive depth increases, the pressure-resistant structure of the submersible is elastically deformed due to the change in water discharge. The balance between gravity and buoyancy is broken due to the increase in weight after sampling the submersible, or the decrease in weight after other equipment is released. Pilot operated hydraulic control valves are utilized to regulate the flow and pressure of the system to ensure that the submersible operates at a relatively stable attitude within a certain depth.

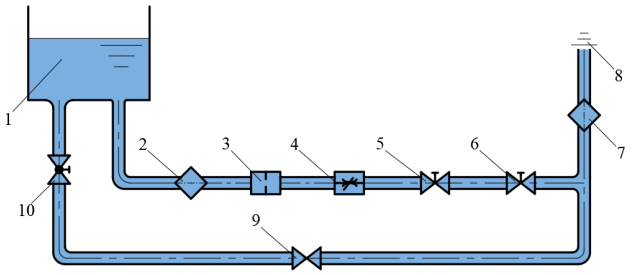

1.Pressure-resistant water chamber 2. Inlet strainer 3. Throttle orifice 4. Pilot-operated hydraulic control valve 5 Regulating valve 6 Globe valve 7. Through-sea filter 8. Seawater 9. Check valve 10. Regulating ball valve

FIGURE 1. Schematic diagram of the buoyancy regulation system for a submersible.

The structure and schematic diagram of a pilot operated hydraulic control valve is shown in Fig.2. Pilot-operated hydraulic control valve senses the pressure in front of the valve through the pilot line, and the action of the pilot valve

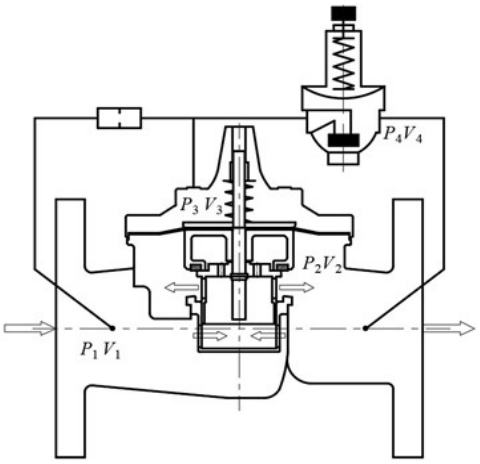

FIGURE 2. Structural model of a pilot-operated hydraulic control valve.

and the main valve can be automatically controlled according to the pressure in front of the valve. Pilot hydraulic control valve adjustable system pressure range of 0.7 $\sim$ 1.6MPa, the valve outlet pressure can be maintained at a lower value, the flow rate design index for 30t/h. When the pre-valve pressure reaches 0.7MPa, the pilot valve according to the valve pressure feedback stabilized in the larger degree of openness, the main valve cavity pressure is far less than the pre-valve pressure, the spool in the pre-valve pressure upward movement, the main valve opening increased. In the pilot-operated hydraulic control valve and system inlet pressure in the process, the pressure after the valve remains unchanged, the flow fluctuations in the design indicators within the deviation.

B. OPERATED HYDRAULIC CONTROL VALVE MATHEMATICAL MODELING

Pilot-operated hydraulic control valve main valve moving assembly force is shown in Fig. 3, the spool motion component is mainly subject to the diaphragm on both sides of the hydraulic pressure difference, spool on both sides of the imbalance force, diaphragm deformation of the rebound force, friction, and liquid viscous damping force. According to the pilot-operated hydraulic control valve main valve structure and operating principle to establish the main spool force balance Equations:

$$F_P = m_1\ddot{x} + B_1\dot{x} + F_s + F_y + F_o + F_f + F_m \qquad (1)$$

In the formula, F_P is the fluid force in the direction of the main valve diaphragm movement, N; F_s is the main valve spring force, N; F_y is the main valve hydrodynamic force, N; F_o is the main valve O-ring friction, N; F_f is the main valve moving component friction, N; F_m is the main valve diaphragm rebound force in the direction of the movement, N; m_1 is the main spool equivalent mass, kg; B_1 is the main spool viscous damping coefficient; x is the main valve spool displacement of the main valve spool, m.

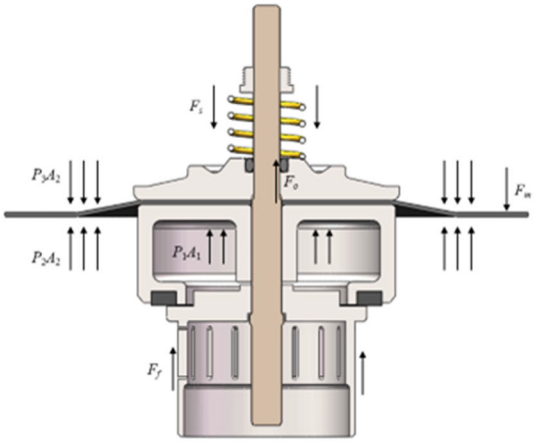

FIGURE 3. Pilot-operated hydraulic control valve main valve moving components force diagram.

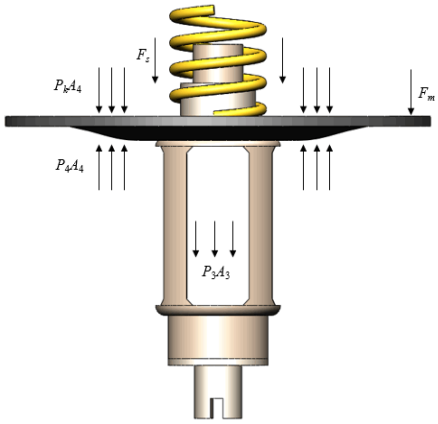

FIGURE 4. Pilot valve moving assembly force analysis diagram.

The fluid force F_P in the direction of the main valve diaphragm movement is:

$$F_P = (P_1 - P_2) A_1 + (P_2 - P_3) A_2 \tag{2}$$

where, A_1 is the main valve spool force area, m^2; A_2 is the main valve diaphragm effective force area, m^2; P_1 is the main valve front pressure, pa; P_2 is the main valve back pressure, pa; P_3 is the pilot chamber pressure, pa.

The friction generated by the O-ring is calculated as:

$$F_o = \frac{f\pi D_o d_o}{1-\mu_o^2}\left[0.2\pi e_o E_o + \mu\left(1+\mu\right)\left(P_3 - P_1\right)\right] \tag{3}$$

where, f is the friction coefficient; d_o is the O-ring cross-section diameter, m; D_o is the O-ring outer diameter, m; e_o is the compression ratio; μ_o is the Poisson's ratio of Buna-N material; E_o is the elastic modulus of Buna-N, Pa.

The friction force F_f of the main valve moving assembly is:

$$F_f = \frac{\left(\tau_d - \tau_c\right)\frac{\omega}{\omega_t}}{\left[\frac{1}{16}\left(\left(\frac{\omega}{\omega_t}\right)^2 + 3\right)^2\right]} + \tau_d \, tanh\left(\frac{4\omega}{\omega_t}\right) \tag{4}$$

where: τ_d and τ_c denote the levels of normalized Coulomb friction and static friction, respectively, ω is the transition velocity of the slip, and ω_t is the characteristic velocity of the dynamic friction;

Equation (1) can be rewritten as:

$$\begin{aligned} m_1\ddot{x} = {} & (P_1 - P_2) A_1 + (P_2 - P_3) A_2 - K_1 (x_0 + x) \\ & - B_1\dot{x} - F_y(x) - F_o - F_f(\dot{x}) \end{aligned} \tag{5}$$

Pilot-operated hydraulic control valve pilot valve moving assembly force shown in Fig. 4, The spool motion component is mainly subject to hydraulic differential force on both sides of the diaphragm, unbalanced force on both sides of the spool, rebound force generated by the deformation of the diaphragm, friction, and liquid viscous damping force.

According to the pilot-operated hydraulic control valve pilot valve structure and operating principle to establish the pilot valve spool force balance equation:

$$F_{P1} = m_2\ddot{y} + B_2\dot{y} + F_{s1} + F_{y1} + F_{m1} \tag{6}$$

where F_{P1} is the fluid force in the direction of pilot valve diaphragm movement, N; F_{s1} is the spring force of the pilot valve, N; F_{y1} is the hydrodynamic force, N; F_{m1} is the rebound force of the pilot valve diaphragm in the direction of movement, N; m_2 is the equivalent mass of the pilot valve spool, kg; B_2 is the viscous damping coefficient of the pilot valve spool; and y is the spool displacement, m.

The fluid force F_{P1} in the direction of motion of the pilot valve diaphragm is:

$$F_{P1} = P_3A_3 + (P_4 - P_k) A_4 \tag{7}$$

where A_3 is the pilot valve spool force area, m^2; A_4 is the effective force area of the pilot valve diaphragm, m^2; P_k is the atmospheric pressure, Pa.

Equation (6) can be written as:

$$\begin{aligned} m_2\ddot{y} = {} & P_3A_3 + (P_4 - P_k) A_4 - B_2\dot{y} - K_2 (y_0 + y) \\ & - F_{y1}(y) - F_{m1}(y) \end{aligned} \tag{8}$$

Pilot-operated hydraulic control valve pressure calculated by the piping system, according to the valve port flow formula for the main valve and pilot valve flow:

$$q_1 = \frac{\pi}{4} C_1 D^2 \sqrt{\frac{2\left(P_1 - P_3\right)}{\rho}} \tag{9}$$

$$q_2 = C_2 \pi D y \, sin\alpha_2 \sqrt{\frac{2\left(P_3 - P_2\right)}{\rho}} \tag{10}$$

where q_1 is the flow through the main valve, t/h; q_2 is the flow through the pilot valve, t/h; C_1 is the main valve orifice flow coefficient; C_2 is the pilot valve orifice flow coefficient; D for the main valve flow cross-section diameter, m; D_y for the pilot valve spool equivalent opening length, m.

The mathematical model of the pilot operated hydraulic control valve is obtained by Laplace transforming the above

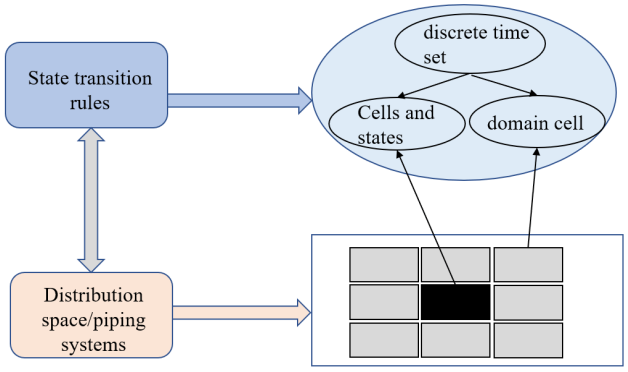

FIGURE 5. Elementary cellular automata.

equations (4), (8), (9) and (10), as shown in (11), at the bottom of the page. Main Valve Port Flow-Displacement Increment:

$$K_{q_1x} = \frac{\partial q}{\partial x} = \frac{1}{4} C_1 \pi D^2 \sqrt{\frac{2\left(P_1 - P_3\right)}{\rho}} \tag{12}$$

Main valve port flow-pressure increment:

$$K_{q_1P} = \frac{\partial q}{\partial P} = \frac{1}{4} C_1 \pi D^2 \sqrt{\frac{2}{\rho}} \frac{1}{\sqrt{2\left(P_1 - P_3\right)}} \tag{13}$$

Pilot valve port flow-displacement increment:

$$K_{q_2y} = C_2 \pi D sin\alpha_2 \sqrt{\frac{2\left(P_3 - P_2\right)}{\rho}} \tag{14}$$

Pilot valve port flow-pressure increment:

$$K_{q_2P} = C_2 \sqrt{\frac{2}{\rho}} A_0\left(y\right) \frac{1}{\sqrt{2\left(P_3 - P_2\right)}} \tag{15}$$

C. -PIPELINE DYNAMICS BASED ON META CELLULAR AUTOMATA TECHNIQUES

A met acellular automaton consists of a cell and its state, a distribution space, a neighborhood radius, and a state transition rule, as shown in Fig. 5, where the evolution rule is a function of the cell itself and its neighboring states. The cell size and time step are determined by the primary temporal and spatial scales of the system under study.

Since the length of the pipeline of the buoyancy adjustment system is large and the change of fluid parameters along the flow direction is more significant than the change of fluid parameters perpendicular to the flow direction, the motion of the pipeline fluid is assumed to be one-dimensional, and the pipeline fluid flow model is regarded as one-dimensional. When the fluid enters the pilot-operated hydraulic control valve from the pipeline before, the system metameric automaton evolves from the beginning to the end. The pressure and flow rate of the beginning metameric cell 1 are P_1 and Q_1 respectively, and the metameric cell 1 is in the reproduction state, the metameric cell 2 is in the growth state, and the rest of the metameric cells are in the idle state. Let a central cell of the system's tuple space be i. Cell $i+1$ is growing and its neighbor is reproducing, then the state of cell $i+1$ at the next moment is the reproducing state, and the cellular automaton evolves as follows:

$$\begin{aligned} a_{i,j}\left(t+1\right) = \big(&f\left(a_{i,j}\right)\left(t\right), a_{i-1,j-1}\left(t\right), a_{i-1,j}\left(t\right), \\ &a_{i-1,j+1}\left(t\right), a_{i,j-1}\left(t\right), a_{i,j+1}\left(t\right), a_{i+1,j}\left(t\right), \\ &a_{i+1,j}\left(t\right), a_{i+1,j+1}\left(t\right)\big) \end{aligned} \tag{16}$$

The derivative of the fluid momentum for time is equal to the sum of the external forces exerted on the micrometric body, The expression for the momentum conservation equation controlling the fluid dynamics in a one-dimensional pipe is given as:

$$\frac{\partial Q_j\left(z,t\right)}{\partial t} + gA\frac{\partial P_j\left(z,t\right)}{\partial x_i} = -\tau Q_j\left(z,t\right)\left|Q_j\left(z,t\right)\right| \tag{17}$$

where: t and z are time and space coordinates, respectively, and A is the cross-sectional area of the pipe.

For a generally cylindrical pipe, the Darcy-Weisbach equation is the classical method used to calculate the pressure loss of the pipe, and its formula for calculating the pressure

$$\begin{cases} \Delta\left(P_1 - P_2\right)A_1 - \Delta\left(P_2 - P_3\right)A_2 = m_1 s^2 \Delta x + B_1 s\Delta x + K_1\Delta x + K_{Ff} + K_{sx}\Delta x + K_{sxP}\Delta P + C_d W_1 h_1\sqrt{2\rho\Delta P}s\Delta x \\ \Delta\left(P_4 - P_k\right)A_4 + \Delta P_3 A_3 = m_2 s^2\Delta y + B_2 s\Delta y + K_2\Delta y + K_{sy}\Delta y + K_{syP}\Delta P + K_{Ff} \\ K_{q_1x}\Delta x + K_{q_1P}\Delta P - \left(K_{q_3x}\Delta x + K_{q_3P}\Delta P\right) = \dfrac{V_1}{E}s\Delta P' - A_1 s\Delta x \\ \left(K_{q_2y} - K_{q_4y}\right)\Delta x + \left(K_{q_2P} - K_{q_4P}\right)\Delta P = A_2 s\Delta x - \dfrac{V_3}{E}s\Delta P_3 \\ \Delta q_v - \left(K_{q_1x}\Delta x + K_{q_1P}\Delta P + K_{q_4y}\Delta x + K_{q_4P}\Delta P\right) = \dfrac{V_1}{E}s\Delta P_1 \end{cases} \tag{11}$$

drop of the fluid flow in the pipe is given by:

$$\Delta P = \lambda \frac{L}{D} \frac{\rho v^2}{2} \tag{18}$$

where ΔP is the pipeline fluid flow pressure drop; λ is the along-track resistance coefficient; L is the length of the pipeline; D is the diameter of the pipeline; ρ is the density of the medium; and v is the average flow rate of the pipeline medium.

Considering that the piping system has damping characteristics, to introduce dynamics, we need to add the corresponding unit transformation rules, and the modified local rules are suggested as follows:

$$R\left(x_i, t_{j+1}\right) = \frac{m\left(\sum_{i=1}^{n} \sum_{j=1(j\neq i)}^{n} \omega\left(x_i + d_{x_{i+1}}, t_j\right) - 2\omega\left(x_i, t_j\right)\right)}{2} + (1-\alpha) R\left(x_i, t_j\right) \tag{19}$$

x_i is the ith cell; t_j is the jth time step; R is the amplitude decay rate; ω is the dynamic response amplitude; α is a constant value describing the damping effect; m is a computational constant; and $d_{x_{i+1}}$ is the cell unit length.

Depending on the different growth states of the metameres of the system pipeline, the metameres states and metameres properties are updated over time. For each position (i, j) in the pipe state matrix, the pressure attribute values are:

$$P_{i+1}^{t+1} = \frac{a_{i+1}}{z_{i+1}} \left[\frac{a_i}{z_i} \left(P_i^t - P_{i+1}^{t+1}\right) - \lambda Q_i^t \left|Q_i^t\right| - \frac{a_i}{L - \sum_{i=1}^{n} z_i} P_{i+1}^{t+1} - \lambda Q_{i+1}^{t+1} \left|Q_{i+1}^{t+1}\right| \right] \tag{20}$$

where: $a_i = gA$, $a_{i+1} = \frac{b^2}{gA}$.

D. -DIMENSION LESSNESS OF THE DYNAMIC MODEL

The spool is in small opening when the system is in large differential pressure, and the spool may collide with the valve seat when it is in unstable state, assuming that the collision is non-perfectly elastic, the spool velocity in this case can be expressed as:

$$\dot{x}^+ = -r\dot{x}^- \ (x = 0, \dot{x} < 0) \tag{21}$$

where, $\dot{x}^+$ is the velocity after the collision, m/s; $\dot{x}^-$ is the velocity before the collision, m/s; r is the collision recovery coefficient.

The obtained nonlinear dynamics equation is transformed into the system state equation, which is expressed in ordinary differential form as follows:

$$\begin{cases} \dot{x} = v_x \\ \dot{v}_x = \dfrac{(p_1 - p_2) A_1 + (p_2 - p_3) A_2}{m_1} - \dfrac{p_1 x C_{d1} \pi D_1}{m_1} - \dfrac{k\left(x + x_0\right)}{m_1} - \dfrac{F_f}{m_1} - \dfrac{B_1 \dot{x}}{m_1} \\ \dot{P} = \dfrac{E}{V}\left[Q_P - C_d A\left(x\right) w\left(p, \dot{x}\right)\right] \\ \dot{x}^+ = -r\dot{x}^- \end{cases} \tag{22}$$

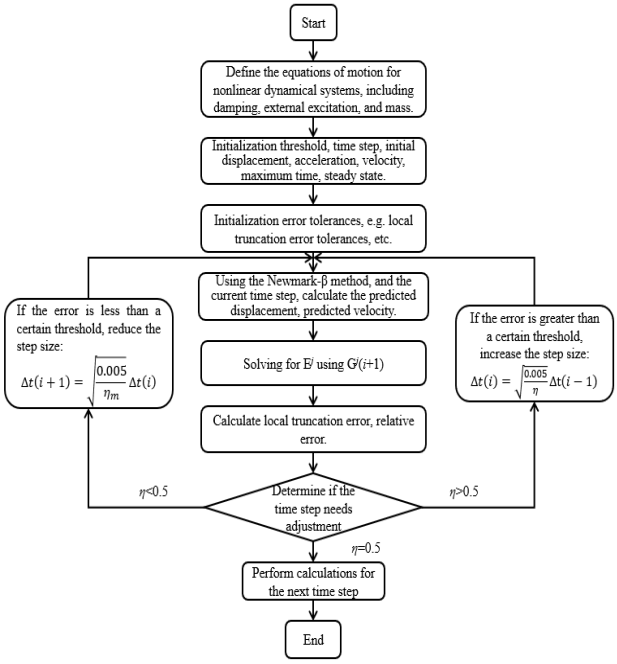

FIGURE 6. Flowchart of the improved Newmark-β integration algorithm.

Before the stability analysis of the established dynamic model, to facilitate the assessment of the system stability, simplify the calculation and eliminate the differences in the order of magnitude of each parameter, the appropriate variables are selected, and the corresponding non-depersonalization is carried out by using the similarity criterion to derive the dimensionless equations. The intrinsic frequency θ_0, the reference time t_r, and the reference displacement x_r are the three basic reference parameters of the dynamic model, which are defined as follows:

$$\theta_0 = \sqrt{\frac{k_1}{m_1}}, \quad t_r = \sqrt{\frac{m_1}{k_1}}, \ x_r = \frac{A_{dx} P_b}{k_1} \tag{23}$$

Based on the three basic reference parameters defined above, the following dimensionless variables can be defined:

$$\begin{cases} e_1 = \dfrac{x}{x_r} = \dfrac{x k_1}{A_d p_b}, & \tau = \dfrac{t}{t_r} = t\sqrt{\dfrac{k_1}{m_1}} \\ e_2 = \dfrac{t_r}{x_r} v_x = \dfrac{\sqrt{m_1 k_1}}{A_d p_b} v_x, & e_3 = \dfrac{P}{p_b} \end{cases} \tag{24}$$

Substituting each dimensionless parameter into Eq. (22), the dimensionless system state equation set is obtained as:

$$\begin{cases} e_1' = e_2 \\ e_2' = \eta - \delta - \gamma - e_1 - \xi e_3 \\ e_3' = \vartheta - \chi\sqrt{e_3} \\ e_2^+ = -r e_2^- \end{cases} \tag{25}$$

Define the new dimensionless parameters such as damping ratio, spring pre-compression coefficient ratio, and system

TABLE 1. Comparison of each algorithm.

Algorithm	Maximum calculation error	Computational efficiency
Runge-Kuta	4.52E-06	99.45
Newmark-β	3.81E-06	92.67
Wilson-θ	5.69E-06	185.65
improved Newmark-β	2.42E-06	65.38

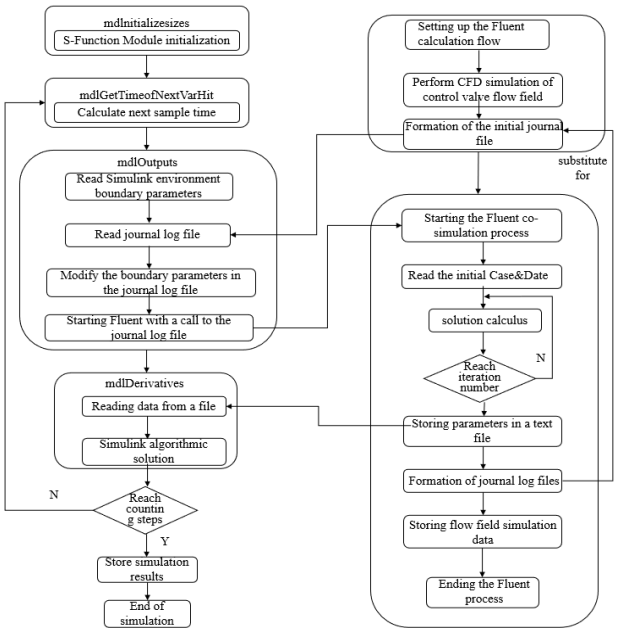

FIGURE 7. MATLAB/Simulink and Fluent Co-simulation Platform Implementation Methods.

stiffness ratio:

$$\eta = \frac{(p_1 - p_2)A_1 + (p_2 - p_3)A_2 - p_1 x C_{d1}\pi D_1}{A_d p_b},$$
$$\delta = \frac{k_1 x_0}{A_d p_b}, \quad \gamma = \frac{F_f}{A_d p_b}, \xi = \frac{B_1}{\sqrt{k_1 m_1}}$$
$$\vartheta = \frac{EQ_P}{VP_b}\sqrt{\frac{m_1}{k_1}}, \quad \chi = \frac{E}{V}C_{d1}A_x\sqrt{\frac{2m_1}{\rho k_1 P_b}} \tag{26}$$

III. IMPROVED ALGORITHM FOR SOLVING NONLINEAR DYNAMICS BY NEWMARK-*β* INTEGRATION METHOD

The Newmark-β method is a commonly used numerical integration method for solving the time response of nonlinear dynamical systems [25], [26], [27]. The basic idea is to adopt the linear acceleration assumption and divide the calculation of acceleration into two steps: predicted acceleration and corrected acceleration. Then, the numerical solutions of displacement and velocity are obtained by iterative solving. However, in practice, the Newmark-β method may suffer from numerical instability and poor accuracy due to the presence of nonlinear effects. Therefore, the time step can be dynamically adjusted by introducing the time step adaptivity, and different time steps can be used in different periods to improve the accuracy and stability of numerical computation.

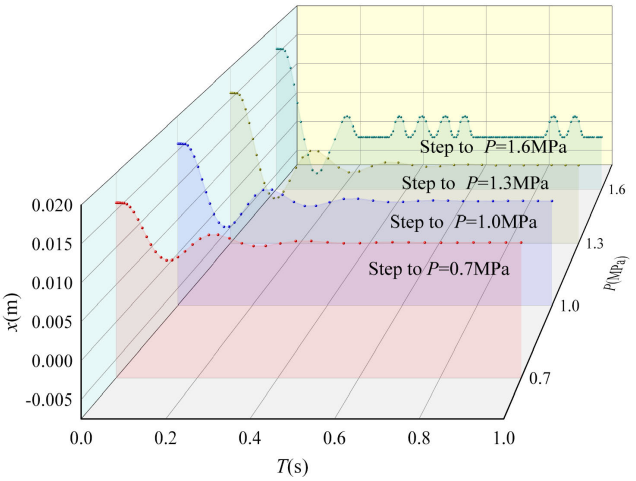

FIGURE 8. Spool motion trajectories on time series for system inlet pressures of 0.7 MPa, 1.0 MPa, 1.3 MPa, 1.6 MPa.

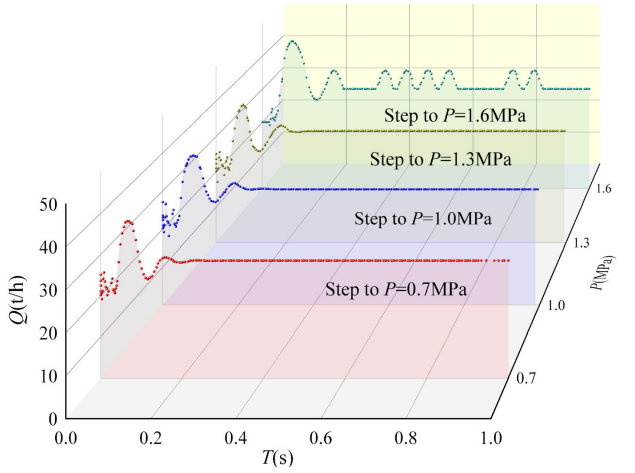

FIGURE 9. System flow rate change curve on time series when the system inlet pressure is 0.7Mpa, 1.0MPa, 1.3MPa, 1.6MPa.

Fig. 6 shows the flowchart of the algorithm for the improved Newmark-β integration method to obtain the nonlinear dynamic bifurcation behavior of the pilot-operated pressure-reducing valve.

$$m\ddot{v}(i+1) + c\dot{v}(i+1) + Ev(i+1) = G^j(i+1) \tag{27}$$

where E is a numerical matrix storing the results of each iteration step under the external excitation. i denotes the number of recurrences and j denotes the number of iterations. The displacement dependence of the nonlinear external force determines the initial guess displacement v_x, which is used to start the algorithm program.

$$E^j v_x(i+1) = Ge^j(i+1) \tag{28}$$

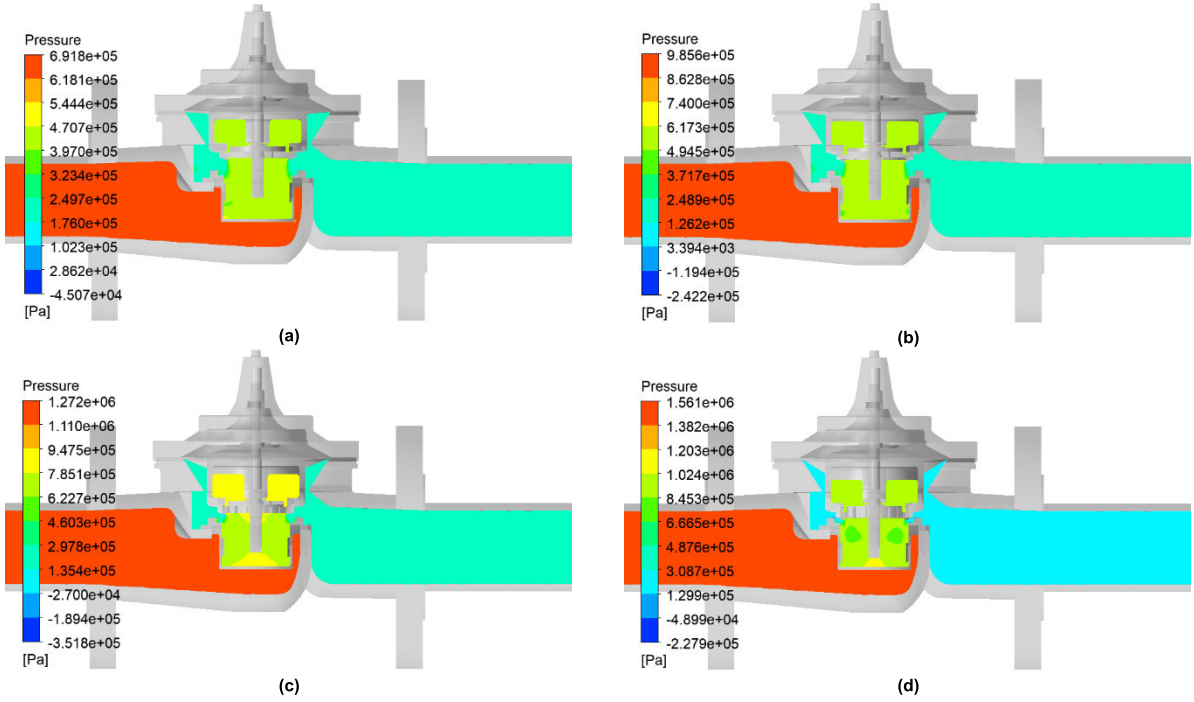

FIGURE 10. System flow rate change curve on time series when the system inlet pressure is 0.7Mpa, 1.0MPa, 1.3MPa, 1.6MPa.

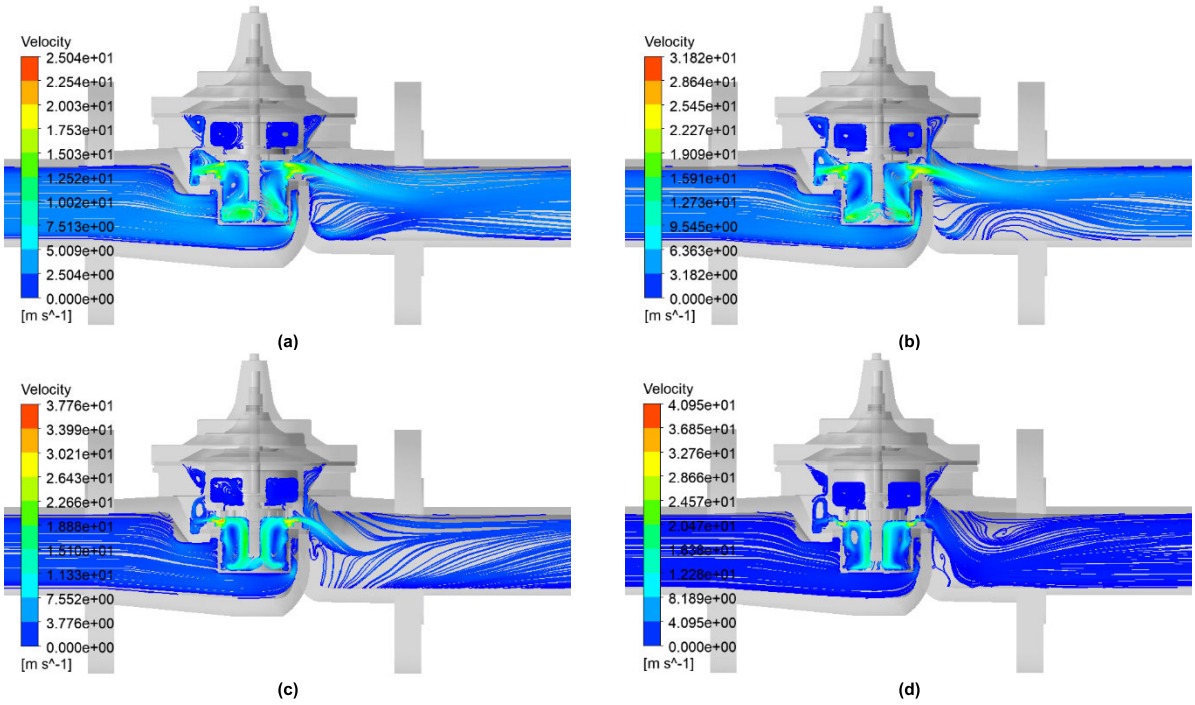

FIGURE 11. Velocity line cloud at different system inlet pressures. (a) P = 0.7 MPa; (b) P = 1.0 MPa; (c) P = 1.3MPa; (d) P = 1.6MPa.

The payload is solved for:

$$Ge^{j}(i+1) = G^{j}(i+1) + \Omega(i) + \Sigma(i) \tag{29}$$

where:

$$\Sigma(i) = M\left[\alpha_1 v(i) + a_3\dot{v}(i) + a_4\ddot{v}(i)\right] \tag{30}$$

$$\Omega(i) = C\left[\lambda a_2 v(i) + a_5\dot{v}(i) + a_6 dt\ddot{v}(i)\right] \tag{31}$$

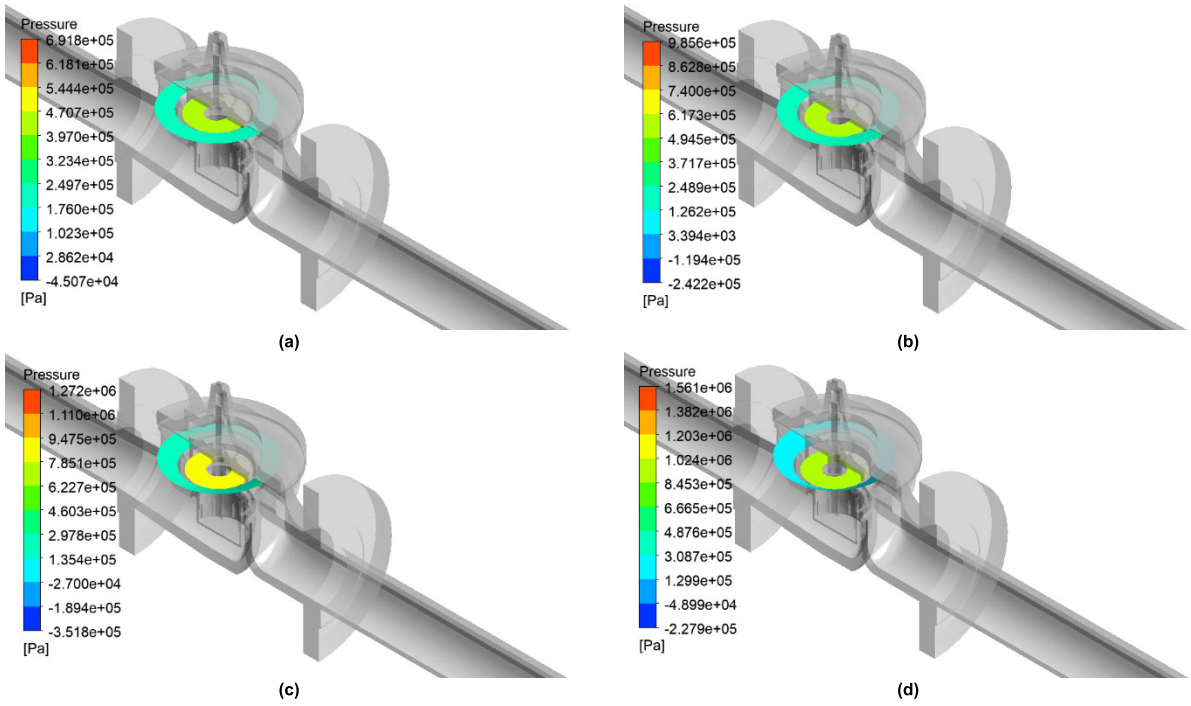

FIGURE 12. Clouds of media force at the monitoring surface at different system inlet pressures. (a) $P = 0.7$ MPa; (b) $P = 1.0$ MPa; (c) $P = 1.3$MPa; (d) $P = 1.6$M.

where: α_1, α_2, α_3, α_4, α_5, and α_6 are the integration variables in the variable step-size integration algorithm, β is the weighting factor for acceleration, and λ is the weighting factor for velocity, which needs to be initialized after each recursion to initialize the step size or tolerance.

$$a_1 = \frac{1}{\beta\,(\Delta t)^2}, \quad a_2 = a_3 = \frac{1}{\beta \Delta t}, \; a_4 = \frac{1}{2\beta} - 1$$
$$a_5 = \frac{\lambda}{\beta} - 1, \quad a_6 = \frac{1}{2}(\frac{\lambda}{\beta} - 1) - \frac{1}{2} = \frac{1}{2}a_5 - \frac{1}{2} \tag{32}$$

The velocity and acceleration are solved for the moment $t + \Delta t$:

$$\dot{v}(i+1) = \frac{1}{\beta \Delta t}\,[v(i+1) - v(i)] - (\frac{\lambda}{\beta} - 1)\dot{v}(i) - (\frac{1}{2}a_5 - \frac{1}{2})\ddot{v}(i) \tag{33}$$

$$\ddot{v}(i+1) = \frac{1}{\beta\,(\Delta t)^2}\,[v(i+1) - v(i)] - \frac{1}{\beta \Delta t}\dot{v}(i) - (\frac{1}{2\beta} - 1)\ddot{v}(i) \tag{34}$$

The step size is controlled by local truncation error, which increases the step size when the local error is too small and shrinks the step size when the local error is too large, to achieve the adaptive control of the step size and control the error within a certain range to improve the accuracy and stability of the numerical calculation.

The local error of Newmark-β can be calculated by the following formula:

$$e_{i+1} = v^*(i+1) - v(i+1) \tag{35}$$

where: e_{i+1} is the local error, $v^*(i+1)$ is the exact solution at $i+1$, $v(i+1)$ is the computed displacement at $i+1$, and the local truncation error is:

$$R_e = M(i+1)\ddot{v}(i+1) + C(i+1)\dot{v}(i+1) + E(i+1)v(i+1) - E^j v_x(i+1) \tag{36}$$

The relative localization error is:

$$\eta = \frac{v^*(i+1) - v(i+1)}{v^*(i+1)} = \frac{(Pe - \frac{1}{6})\dddot{v}(i)\Delta t^3}{v(i) + \dot{v}(i)\Delta t + \frac{1}{2}\ddot{v}(i)\Delta t^2 + \frac{1}{6}\dddot{v}(i)\Delta t^3} \tag{37}$$

At the present to carry out the bifurcation of the pilot-operated hydraulic control valve, it is defined as follows: when η >0.5 reduce the step size and recalculate the result, currently the step size is:

$$\Delta t(i) = \sqrt{\frac{0.005}{\eta}}\,\Delta t(i-1) \tag{38}$$

Increase the step size when $\eta < 0.5$ and use the new step size in subsequent calculations, when the compensation is:

$$\Delta t(i+1) = \sqrt{\frac{0.005}{\eta_m}}\,\Delta t(i) \tag{39}$$

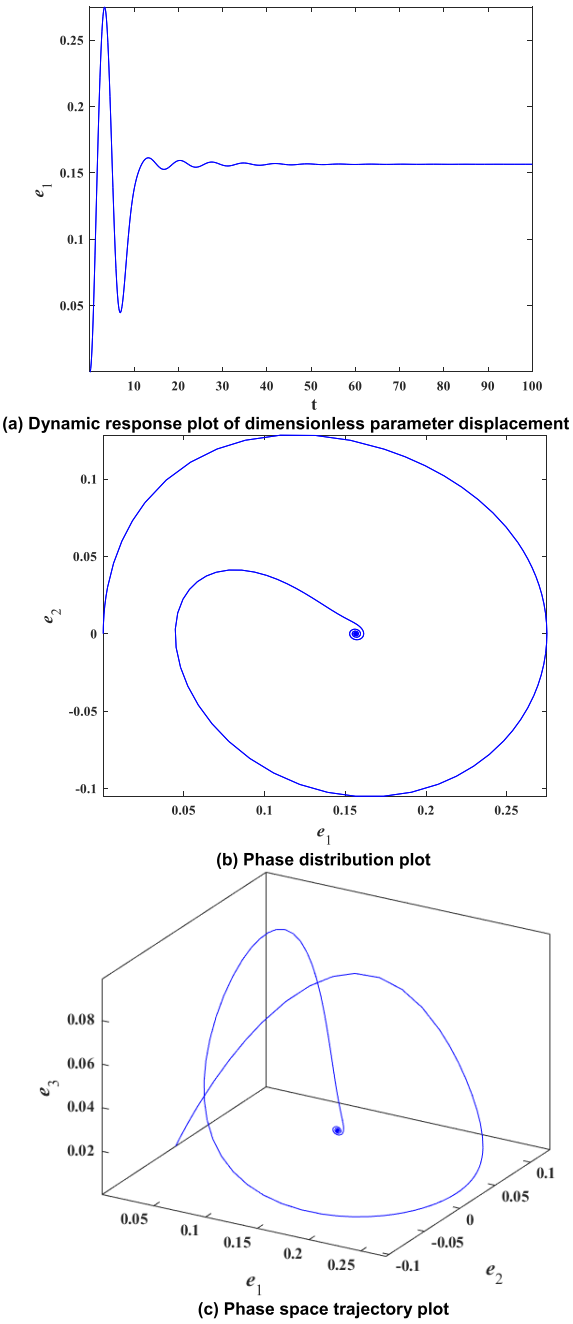

FIGURE 13. Dynamic response plot of nonlinear system ($\eta = 0.2$).

where η_m is the maximum relative error and Pe is the control parameter.

For the nonlinear system studied in this paper, the *Runger-Kutta* method tends to diverge at longer integration times. The improved Newmark-β method proposed in this paper improves the computational convergence while ensuring the solution speed.

In the traditional numerical calculation methods, the simultaneous introduction of multiple nonlinear factors may lead to divergence of the calculation results. It is impossible to accurately evaluate the nonlinear dynamical bifurcation

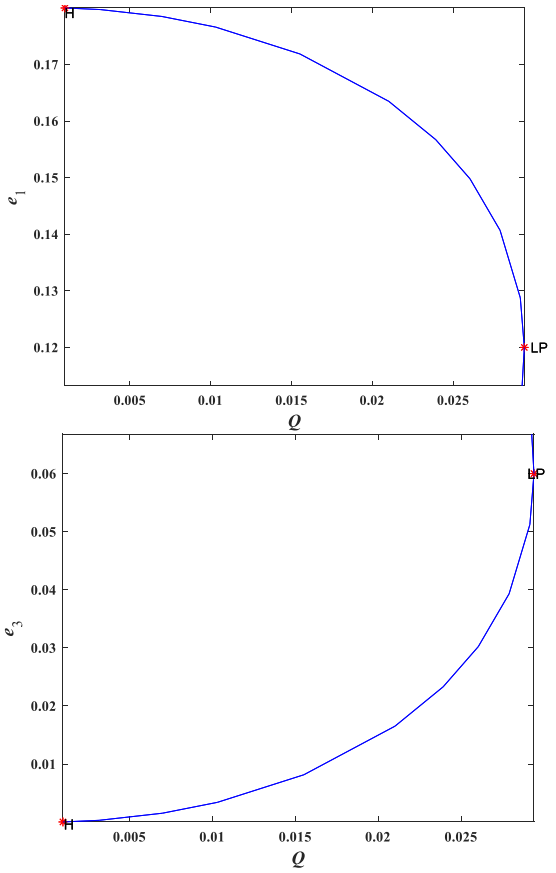

FIGURE 14. Single-parameter bifurcation diagram ($\eta = 0.2$, Q is a free parameter).

behavior. As shown in table1, The Newmark-β integration method proposed in this paper effectively solves the problems existing in the traditional numerical calculation methods.

IV. NONLINEAR DYNAMIC BEHAVIOR ANALYSIS OF PILOT-OPERATED PRESSURE REDUCING VALVE

A. JOINT SIMULATION ANALYSIS OF DYNAMIC CHARACTERISTICS OF PILOT-OPERATED HYDRAULIC CONTROL VALVE

When the system inlet pressure changes from 0.2MPa to 0.7MPa, 1.0MPa, 1.3MPa, and 1.6MPa, the S function is used to compile the MATLAB/Simulink and Fluent co-simulation data interaction interface program [28], and one and three-dimensional co-simulation platforms are established for the pilot-operated hydraulic control valve portion of the system, and the specific implementation of its joint simulation is shown in Fig. 7.

As shown in Fig. 7, under the MATLAB/Simulink simulation environment, the spool displacement trajectory and the system flow rate change curve are obtained, as shown in Figs. 8 and 9.

As shown in Figs. 8 and 9, when the system inlet pressure changes from 0.2MPa to 0.7MPa, the system flow rate

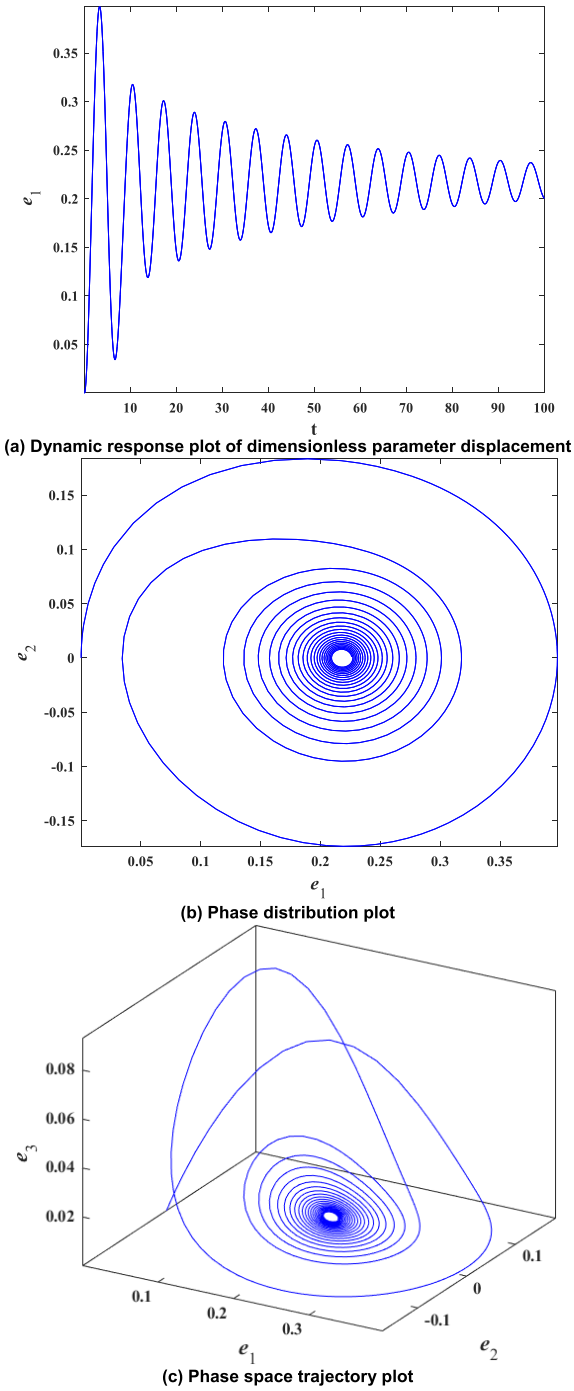

FIGURE 15. Dynamic response plot of nonlinear system ($\eta = 0.25$).

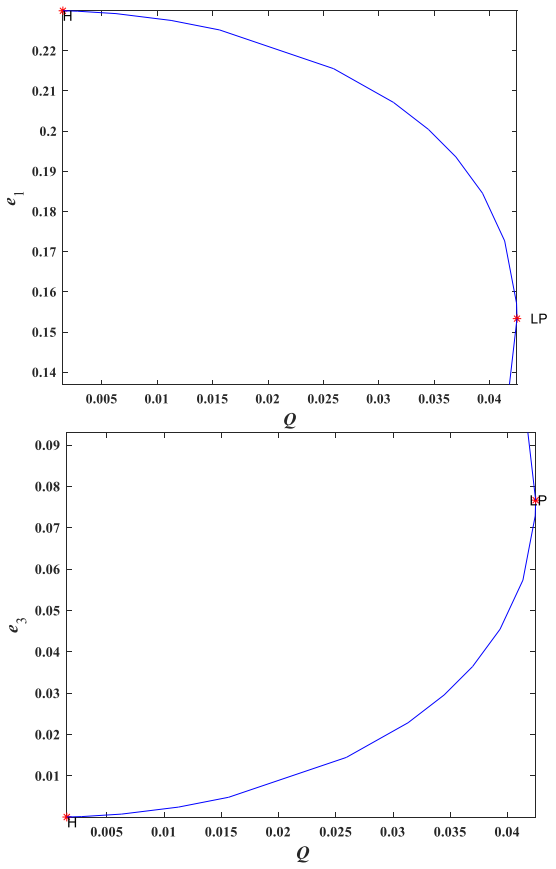

FIGURE 16. Single-parameter bifurcation diagram ($\eta = 0.25$, Q is a free parameter).

stabilizes to 29.65t/h; when the system inlet pressure steps from 0.2MPa to 1.0MPa, the system flow rate stabilizes to 30.41t/h; when the system inlet pressure steps from 0.2MPa to 1.3MPa, the system flow rate stabilizes to As the system inlet pressure increases, the system dynamic response time increases and the system flow rate stabilization value increases. When the system inlet pressure changes from 0.2MPa to 1.6MPa, the initial stabilized value of the system flow rate is 31.85t/h. With the growth of time, the system flow rate value will fluctuate and oscillate, and the flow rate cannot reach constant.

As shown in Figs. 10-12, the results of the transient flow field of the UDF dynamic grid at different moments in FLUENT under the system inlet pressures of 0.7 MPa, 1.0 MPa, 1.3 MPa, and 1.6 MPa.

B. ANALYSIS OF SYSTEM NONLINEAR DYNAMIC BEHAVIOR

In section A, the preliminary calculations of flow values and spool trajectories under different system inlet pressures are carried out, and the results show that when the system inlet pressure is 1.6MPa, the system flow rate changes irregularly, and it is impossible to analyze it by the dynamic characteristics. In this section, we will take Q as a free parameter, and take the system inlet pressure of 1.6MPa and the flow rate of 29.94t/h as the initial parameter, and based on the nonlinear dynamic system, calculate the system to get the phase and vector field distribution diagrams of different parameters, and study the stability and dynamic response characteristics of the pilot-operated hydraulic control valve dynamic system under different regulating parameters, calculate and draw the bifurcation diagram to analyze the bifurcation characteristics and stability of the dynamic system.

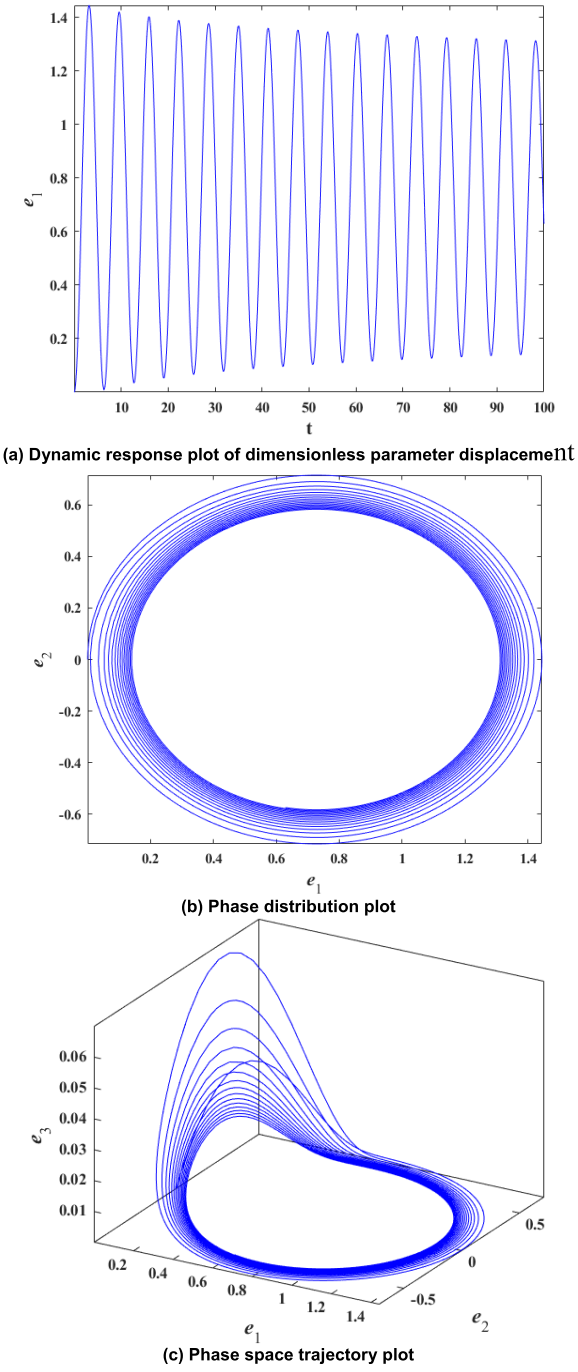

FIGURE 17. Dynamic response plot of nonlinear system ($\eta = 0.75$).

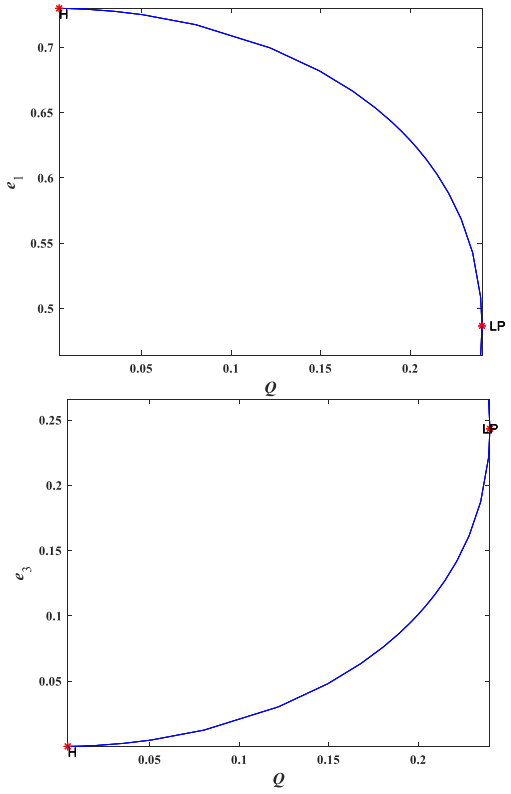

FIGURE 18. Single-parameter bifurcation diagram ($\eta = 0.75$, Q is a free parameter).

As shown in Fig. 13, the system is stable at $\eta = 0.2$, the displacement response curve converges in 50-time steps after many oscillations, and the corresponding phase space trajectory stabilizes at the equilibrium point after many motion cycles.

As shown in Fig. 14 when $\eta = 0.2$, the dimensionless flow parameter is reduced from $Q = 0.03$, and two bifurcation points appear in the system, LP denotes the limit loop saddle knot bifurcation and H denotes the Hopf bifurcation. The limiting ring-saddle knot bifurcation occurs when $Q = 0.029$, with ($e_1 = 0.12$, $e_3 = 0.06$) at the stable equilibrium point; the supercritical Hopf bifurcation occurs when $Q = 0.0003$, with ($e_1 = 0.18$, $e_3 = 3.71 \times 10^{-6}$) at the stable equilibrium point. In the interval $Q \in (0.0003, 0.029)$, there are two stability states, the limit ring motion and the stable equilibrium point. At the saddle-knot bifurcation point, the trajectory line of the system's operation progresses towards another equilibrium point in phase space or diverges towards infinity. At the Hopf bifurcation point, the loss of system stability is due to the interaction of the equilibrium point with the limit ring. In nonlinear systems, Hopf bifurcation is the beginning of the oscillatory phenomenon, where a dynamical system operating at a stable equilibrium point begins to oscillate when the parameters change slowly to the point where a Hopf bifurcation occurs.

As shown in Fig. 15, the system is unstable at $\eta = 0.25$, and the state variables are in an oscillatory response state tending to the limit loop or stabilization point after the system has been subjected to small fluctuations and tends to the limit loop or stabilization point state after some time, and the corresponding phase-space trajectory also shows a tendency to the limit loop or stabilization point state, and enters into the limit loop or stabilization point state after several motion cycles.

As shown in Fig. 16, the dimensionless flow parameter is reduced from $Q = 0.045$. The limit-loop saddle-knot

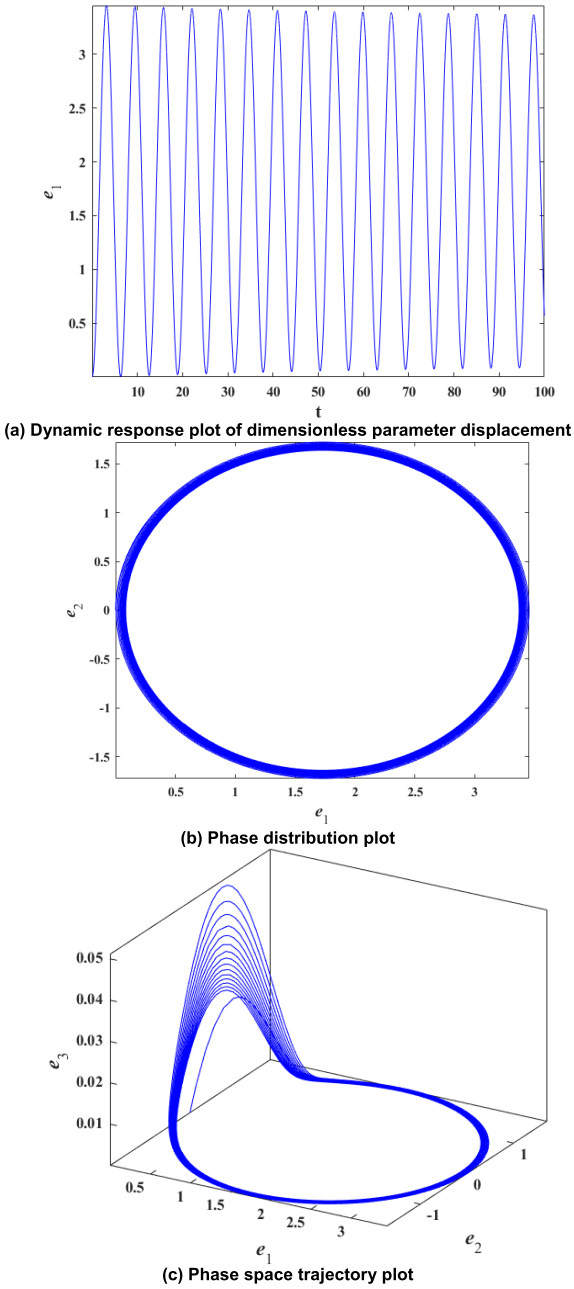

FIGURE 19. Dynamic response plot of nonlinear system ($\eta = 1.75$).

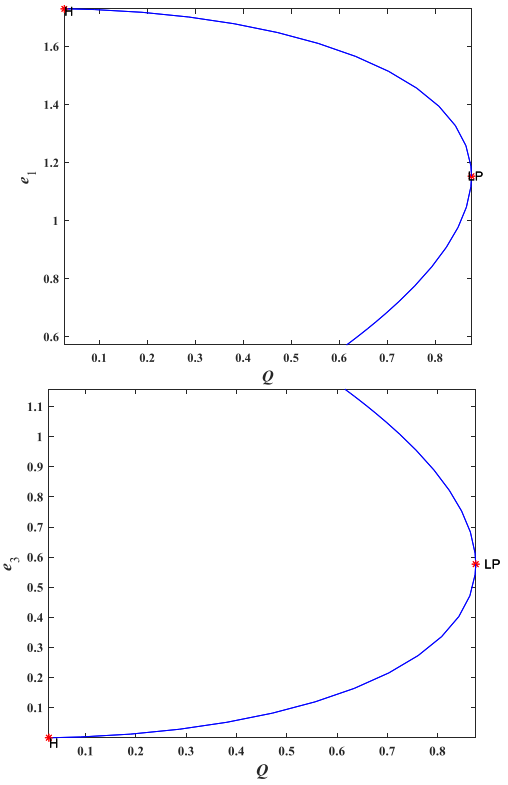

FIGURE 20. Single-parameter bifurcation diagram ($\eta = 1.75$, Q is a free parameter).

bifurcation occurs at $Q = 0.0425$ with ($e_1 = 0.153$, $e_3 = 0.077$) at the stable equilibrium point, and the supercritical Hopf bifurcation occurs at $Q = 0.0015$ with ($e_1 = 0.23$, $e_1 = 4.2\times10^{-5}$) at the stable equilibrium point. In the interval $Q \in (0.0015, 0.0425)$, there are two stability states, the limit ring motion, and the stable equilibrium point.

As shown in Fig. 17, the system is unstable at $\eta = 0.75$, and the state variables are first in an oscillatory response state after the system is subjected to small fluctuations and converge to the limit-loop state after a period, and the corresponding phase-space trajectories also show convergence to the limit-loop state, and enter the limit-loop state after several motion cycles.

As shown in Fig. 18, the dimensionless flow parameters are reduced from $Q = 0.25$. The limit-loop saddle-knot bifurcation occurs at $Q = 0.24$ with ($e_1 = 0.487$, $e_3 = 0.243$) at the stable equilibrium point, and the supercritical Hopf bifurcation occurs at $Q = 0.004$ with ($e_1 = 0.73$, $e_3 = 3.11 \times 10^{-5}$) at the stable equilibrium point. In the interval $Q \in (0.004, 0.24)$, there exists a state of limit ring motion.

As shown in Fig. 19, at $\eta = 1.75$, the response state of the state variables after the system is subjected to a small fluctuation is approximately equal amplitude oscillation, and the phase space trajectory of the system exhibits a stable limit loop.

As shown in Fig. 20, the dimensionless flow parameter is reduced from $Q = 0.9$. The limit loop saddle-node bifurcation occurs at $Q = 0.876$ with ($e_1 = 1.153$, $e_3 = 0.577$) at the stable equilibrium point, and the supercritical Hopf bifurcation occurs at $Q = 0.027$ with ($e_1 = 1.73$, $e_3 = 2.44 \times 10.4$) at the stable equilibrium point. In the interval $Q \in (0.027, 0.876)$, there exists a state of limiting ring motion.

V. CONCLUSION

In this study, the buoyancy adjustment system and pilot hydraulic control valve of a submersible are modeled.

A high-precision numerical simulation method considering both the one-dimensional system and the three-dimensional flow is developed. The dynamic characteristics of the system are investigated by combining the meta-cellular automata technique. An improved Newmark-β integration method is proposed to solve the model in the long-time domain. The system is also analyzed for stability by using displacement dynamic response diagrams, phase space trajectory diagrams, and bifurcation diagrams.

1.Through the establishment of a joint simulation model combining MATLAB/Simulink and UDF dynamic mesh. The flow rate change curves of the system under different system inlet pressures and the spool trajectories with time are simulated. The results show that when the system inlet pressure is 1.6MPa, the system flow rate will fluctuate and oscillate after stabilizing for a period, and the flow rate cannot reach constant.

2.MATLAB/Matcont is used to draw the dynamic response diagram and stability analysis of the system. The results show that, with the increase of the pressure in front of the valve, the buoyancy adjustment system undergoes the four states of convergence, large attenuation oscillations, small attenuation oscillations, and equal-amplitude oscillations. And all of them are converging to the equilibrium point and the limit ring in the two forms of stabilization.

3.The nonlinear dynamic behavior of the system is investigated by the improved Newmark-β integration method. The results show that when the inlet pressure of the system is 1.6MPa, the pressure in front of the valve will have a large step when the piping system is disturbed and unstable phenomena such as water hammer occurs, at which time the stability of the dynamic system changes.

4.In the system inlet pressure of 1.6MPa, as the hydraulic control valve pre-valve pressure increases, there will be a limit loop saddle knot bifurcation and supercritical Hopf bifurcation, bifurcation process produces a limit loop frequency just close to the oscillation of the intrinsic frequency, which is the main reason for the production of flow fluctuations and jump phenomena, for the application of the nonlinear system bifurcation theory in terms of the self-powered valves to provide the direction of the application of research.

REFERENCES

[1] Z. Li, X. Ma, Y. Li, Q. Meng, and J. Li, "ADRC-ESMPC active heave compensation control strategy for offshore cranes," *Ships Offshore Struct.*, vol. 15, no. 10, pp. 1098–1106, Nov. 2020.

[2] Z. Wang, Y. Liu, Q. Cheng, H. Pang, Y. Ma, S. Zhao, W. Wang, and D. Wu, "Dynamic characteristics evaluation of balance valve for seawater hydraulic variable ballast system considering the depth variation," *Ships Offshore Struct.*, vol. 2022, pp. 1–11, Dec. 2022.

[3] Z. Shang, W. Ruan, H. Qiao, and Y. Bai, "Study on risk assessment and numerical simulation method of subsea manifold system," *Ships Offshore Struct.*, vol. 16, pp. 245–255, Aug. 2021.

[4] H. Awad and J. Parrondo, "Nonlinear dynamic performance of the turbine inlet valves in hydroelectric power plants," *Adv. Mech. Eng.*, vol. 15, no. 1, Jan. 2023, Art. no. 168781322211452.

[5] S. Yin, T. Yin, Z. Hu, and X. Liu, "The analysis in dynamic characteristics for check valve of water micro-piston pump," in *Proc. IEEE 8th Int. Conf. Fluid Power Mechatronics (FPM)*, Apr. 2019, pp. 1307–1312.

[6] L. G. Kozlov, L. K. Polishchuk, and O. V. Piontkevych, "Experimental research characteristics of counterbalance valve for hydraulic drive control system of mobile machine," *Przegld Elektrotechniczny*, vol. 95, no. 4, pp. 104–109, 2019.

[7] C. Cui, S. Jiang, X. He, K. Wang, H. Shao, and Z. Wu, "Experimental study on the location of gas drainage pipeline leak using cellular automata," *J. Loss Prevention Process Industries*, vol. 56, pp. 68–77, Nov. 2018.

[8] K. U. Yang, J. G. Hur, G. J. Kim, and D. H. Kim, "Non-linear modeling and dynamic analysis of hydraulic control valve; effect of a decision factor between experiment and numerical simulation," *Nonlinear Dyn.*, vol. 69, no. 4, pp. 2135–2146, Sep. 2012.

[9] D. Mua, C. Xub, and Z. Liua, "Further insight into bifurcation and hybrid control tactics of a chlorine dioxide-iodine-malonic acid chemical reaction model incorporating delays," *MATCH Commun. Math. Comput. Chem.*, vol. 89, no. 3, pp. 529–566, 2023.

[10] C. Xu, Z. Liu, P. Li, J. Yan, and L. Yao, "Bifurcation mechanism for fractional-order three-triangle multi-delayed neural networks," *Neural Process. Lett.*, vol. 55, no. 5, pp. 6125–6151, Oct. 2023.

[11] P. Li, Y. Lu, C. Xu, and J. Ren, "Insight into Hopf bifurcation and control methods in fractional order bam neural networks incorporating symmetric structure and delay," *Cognit. Comput.*, vol. 2023, pp. 1–43, May 2023.

[12] C. Xu, Q. Cui, Z. Liu, Y. Pan, X. Cui, W. Ou, M. U. Rahman, M. Farman, S. Ahmad, and A. Zeb, "Extended hybrid controller design of bifurcation in a delayed chemostat model," *MATCH Commun. Math. Comput. Chem.*, vol. 90, no. 3, pp. 609–648, 2023.

[13] P. Li, X. Peng, C. Xu, L. Han, and S. Shi, "Novel extended mixed controller design for bifurcation control of fractional-order Myc/E2F/miR-17–92 network model concerning delay," *Math. Methods Appl. Sci.*, vol. 46, no. 18, pp. 18878–18898, Dec. 2023.

[14] C. Bazsó, A. R. Champneys, and C. J. Hös, "Bifurcation analysis of a simplified model of a pressure relief valve attached to a pipe," *SIAM J. Appl. Dyn. Syst.*, vol. 13, no. 2, pp. 704–721, Jan. 2014.

[15] G. Licsko, A. Champneys, and C. Hos, "Nonlinear analysis of a single stage pressure relief valve," *IAENG Int. J. Appl. Math.*, vol. 39, no. 4, pp. 286–299, 2009.

[16] C. Gao, X. Yu, H. Nan, C. Men, P. Zhao, Q. Cai, and J. Fu, "Stability and dynamic analysis of doubly-fed variable speed pump turbine governing system based on Hopf bifurcation theory," *Renew. Energy*, vol. 175, pp. 568–579, Sep. 2021.

[17] C. Hos and A. R. Champneys, "Grazing bifurcations and chatter in a pressure relief valve model," *Phys. D, Nonlinear Phenomena*, vol. 241, no. 22, pp. 2068–2076, Nov. 2012.

[18] S. Liu, H. Ai, Z. Pang, Z. Lin, and D. Zhao, "Hopf bifurcation control of nonlinear electromechanical coupling main drive system of rolling mill," *Eur. Phys. J. Plus*, vol. 135, no. 4, pp. 1–14, Apr. 2020.

[19] M. Liao, Y. Zheng, Z. Gao, and W. Song, "Fluid-structure coupling modelling and parameter optimization of a direct-acting relief valve for underwater application," *Nonlinear Dyn.*, vol. 105, no. 4, pp. 2935–2958, Sep. 2021.

[20] W. Ma, W. Song, and L. Qiu, "Instability analysis of pressure relief valve based on Lyapunov exponent and non-smooth bifurcation theory," *J. Appl. Sci. Eng.*, vol. 22, no. 2, pp. 329–336, 2019.

[21] D. Wang, Y. Yin, J. Fu, and H. Jian, "Effect of the balanced piston on the stability of hydraulic pilot-operated relief valve," *Proc. Inst. Mech. Eng., C, J. Mech. Eng. Sci.*, vol. 237, no. 2, pp. 321–334, 2023.

[22] H. Jian, M. Du, and H. Gu, "Modeling and bifurcation analysis of a hydraulic actuator system with different valve spool geometry," *Adv. Mech. Eng.*, vol. 14, no. 8, Aug. 2022, Art. no. 168781322211184.

[23] W. Wei, H. Jian, Q. Yan, X. Luo, and X. Wu, "Nonlinear modeling and stability analysis of a pilot-operated valve-control hydraulic system," *Adv. Mech. Eng.*, vol. 10, no. 11, Nov. 2018, Art. no. 168781401881066.

[24] O. Gad, "Comprehensive nonlinear modeling of a pilot operated relief valve," *J. Dyn. Syst., Meas., Control*, vol. 135, no. 1, 2013, Art. no. 011011.

[25] Y. Zhao, Y. Liu, X. Xin, S. Yu, H. Ma, and Q. Han, "Dynamic modelling considering nonlinear factors of coupled spur gear system and its experimental research," *IEEE Access*, vol. 8, pp. 84971–84980, 2020.
[26] W. Quan and Q. Chang, "Variable-length cable dynamics of payout and reel-in with a vertically tethered underwater drill rig," *IEEE Access*, vol. 8, pp. 66625–66637, 2020.
[27] B. Li, R. Zhang, B. Zhang, Y. Cui, and Q. Yang, "A new energy recovery device by utilizing the merchant ship rolling," *IEEE Access*, vol. 8, pp. 162049–162065, 2020.
[28] F. Q. Chen, J. Y. Qian, M. R. Chen, M. Zhang, L. L. Chen, and Z. J. Jin, "Turbulent compressible flow analysis on multi-stage high pressure reducing valve," *Flow Meas. Instrum.*, vol. 61, pp. 26–37, Jun. 2018.

SHUXUN LI received the master's degree from the Lanzhou University of Technology. He is currently a Professor and a Ph.D. Supervisor of chemical process machinery with the Lanzhou University of Technology. His research interests include dynamic behavior analysis and fluid dynamics of valves.

YU ZHANG is currently pursuing the master's degree with the School of Petrochemical Engineering, Lanzhou University of Technology. His research interests include dynamic characteristic analysis and nonlinear dynamics studies of valve-controlled piping systems.

CHAO LIAN received the master's degree from the Lanzhou University of Technology, in 2023. He is currently with the Shanghai Institute of Applied Physics. His research interests include the dynamic characterization of valve piping systems and the design of equipment for loop systems.

JIANJUN HOU received the master's degree from the Lanzhou University of Technology, where he is currently pursuing the Ph.D. degree. His research interests include dynamic characteristic analysis and multi-objective optimization of valve-controlled piping systems.